Structural Disorder Determines Capacitance in Nanoporous Carbons

Xinyu Liu,[1] Dongxun Lyu,[1] Céline Merlet,[2,3] Matthew J.A. Leesmith,[4] Xiao Hua,[4] Zhen Xu,[1] Clare P. Grey,[1] Alexander C. Forse[1]*

1 Department of Chemistry, University of Cambridge, Cambridge CB2 1EW, U.K.
2 CIRIMAT, Université Toulouse 3 Paul Sabatier, Toulouse INP, CNRS, Université de Toulouse, 118 Route de Narbonne, Cedex 9, Toulouse 31062, France
3 Réseau sur le Stockage Électrochimique de l'Énergie (RS2E), Fédération de Recherche CNRS 3459, Amiens 80039, France
4 Department of Chemistry, Lancaster University, Lancaster LA1 4YB, U.K.
Corresponding author. Email: acf50@cam.ac.uk

Abstract

The difficulty in characterizing the complex structures of nanoporous carbon electrodes has led to a lack of clear design principles with which to improve supercapacitors. Pore size has long been considered the main lever to improve capacitance. However, our evaluation of a large series of commercial nanoporous carbons finds a lack of correlation between pore size and capacitance. Instead, nuclear magnetic resonance spectroscopy measurements and simulations reveal a strong correlation between structural disorder in the electrodes and capacitance. More disordered carbons with smaller graphene-like domains show higher capacitances due to the more efficient storage of ions in their nanopores. Our findings suggest ways to understand and exploit disorder to achieve highly energy dense supercapacitors.

One Sentence Summary

Local structural disorder is the primary factor for enhanced capacitance in nanoporous carbons.

Main Text

Electrochemical double layer capacitors (EDLCs) are a class of supercapacitor energy storage devices with superior power performances and longer cycle lives than batteries (*1, 2*). The most commonly studied and cheapest EDLCs contain activated carbon electrodes formed from disordered, graphene-like sheets that form a porous network with a distribution of pore sizes (*3*). In order to improve the energy densities of these devices closer towards those of batteries, many studies focus on varying the structure of the nanoporous carbon electrodes (*4*) so as to tune the carbon pore size (as measured by gas sorption). While early studies of titanium carbide-derived carbons (TiC-CDCs) with different pore sizes (*3, 5, 6*), as well as studies of activated carbons (*7*), which are the most commonly used electrode materials in commercial supercapacitors, reported a maximum capacitance as the carbon pore sizes were decreased towards the size of desolvated electrolyte ions (*3, 5-7*), more recent studies have generated contradictory results. For example, a lack of correlation between capacitance and pore size across a collection of porous carbons with pore sizes ranging from 0.7 to 15 nm in a standard NEt_4BF_4 in acetonitrile (ACN) electrolyte, including 22 microporous activated carbons from different precursors, TiC-CDCs, and 6 mesoporous carbons was reported (*8*). Further studies also observed a lack of correlation between the pore size and capacitance (*9-11*), with only a modest increase of 17% observed for pores around 0.75 nm from computational investigations (*12*). These contrasting results have led to unclear design principles for improving EDLC electrodes and suggest that an additional unknown structural variable impacts the capacitance.

Over the past decade, solid-state nuclear magnetic resonance (NMR) spectroscopy has emerged as a probe of both the local chemical structure of EDLC electrodes, as well as their charge storage mechanisms (*13-16*)(*13-20*). NMR spectra of carbons saturated with electrolyte reveal separate resonances for "in-pore" ions (adsorbed in the carbon nanopores) and "ex-pore" ions (located outside the carbon pore network). The in-pore resonance appears at lower chemical shifts than the corresponding neat electrolyte due to the "ring currents" generated by the circulation of delocalized π-electrons in the aromatic carbon rings in the applied magnetic field (*17*). This effect is quantified by the Δδ value, which is defined as:

$$\Delta\delta\ (ppm) = \delta_{in-pore} - \delta_{neat\ electrolyte} \quad (1)$$

Where $\delta_{neat\ electrolyte}$ is the chemical shift of free electrolyte and $\delta_{in-pore}$ is the chemical shift of "in-pore" resonance.

The magnitude of the Δδ value is a measure of the strength of the ring current effect and is therefore a powerful probe of the local structure of the nanoporous carbon, and the "ordered domain size" (*18*), *i.e.,* the average size of the graphene-like fragments that form the carbon pore walls (*18*). Our previous study showed that carbons prepared at lower synthesis temperatures have Δδ values of smaller magnitude due to their smaller ordered domain sizes and more disordered local structures (*18*). The carbon pore size also impacts the magnitude of Δδ, though to a lesser extent, with carbons with smaller pore sizes giving rise to Δδ values of larger magnitude (*19*). Our lattice simulation method enables the extraction of ordered domain sizes from Δδ values by accounting for pore size effects, as well as effects from preferential adsorption of the probe molecules on the carbon surfaces (*20, 21*). The Δδ value measured by NMR spectroscopy is emerging as a probe of structural disorder in nanoporous carbon structures (*18, 22*).

Impact of Porosity on Capacitance

Ten commercially available nanoporous carbons from a range of suppliers were initially selected (see Methods). Analysis of gas sorption data revealed that five had very similar pore size distributions (Fig. 1A, fig. S1, fig S2) and similar specific BET define surface areas (1694-1821 m^2/g, table S1), so these were selected to test whether factors beyond porosity impact capacitance. Despite the similarity in pore size distributions, these five carbons exhibit significantly different capacitance values with a standard NEt_4BF_4 in acetonitrile (1 M) electrolyte, with values ranging from 138 F/g to 83 F/g (Fig. 1B, figs. S3-S5). Measurements at different charging rates (fig. S6), as well as the measurements with ionic liquid electrolytes **(**fig. S7**)**, revealed similar results, with ACS-PC and SC-1800 displaying the highest capacitances and PW-400 displaying the smallest capacitance. Together, these findings suggest that factors beyond pore size and specific surface area impact capacitance.

To explore the impact of porosity further, three commercial activated carbon cloths (ACCs) with significantly different pore size distributions and BET surface areas were studied (Fig. 1C, table S1). These materials demonstrate similar capacitance values, within a range of ~9 F/g (Fig. 1D), suggesting a minor impact of porosity on capacitance for these materials. Combining these results together with a wider series of nanoporous carbon samples including thermally annealed samples (see below, and Methods), no obvious correlation is observed between capacitance and average pore size (Fig. 1E), nor BET surface area (Fig. 1F), suggesting that structural features other than pore size and surface area may govern the capacitance. Finally, oxygen content from X-ray photoelectron spectroscopy (XPS) measurements also did not show a clear correlation with capacitance (fig. S8 table S2).

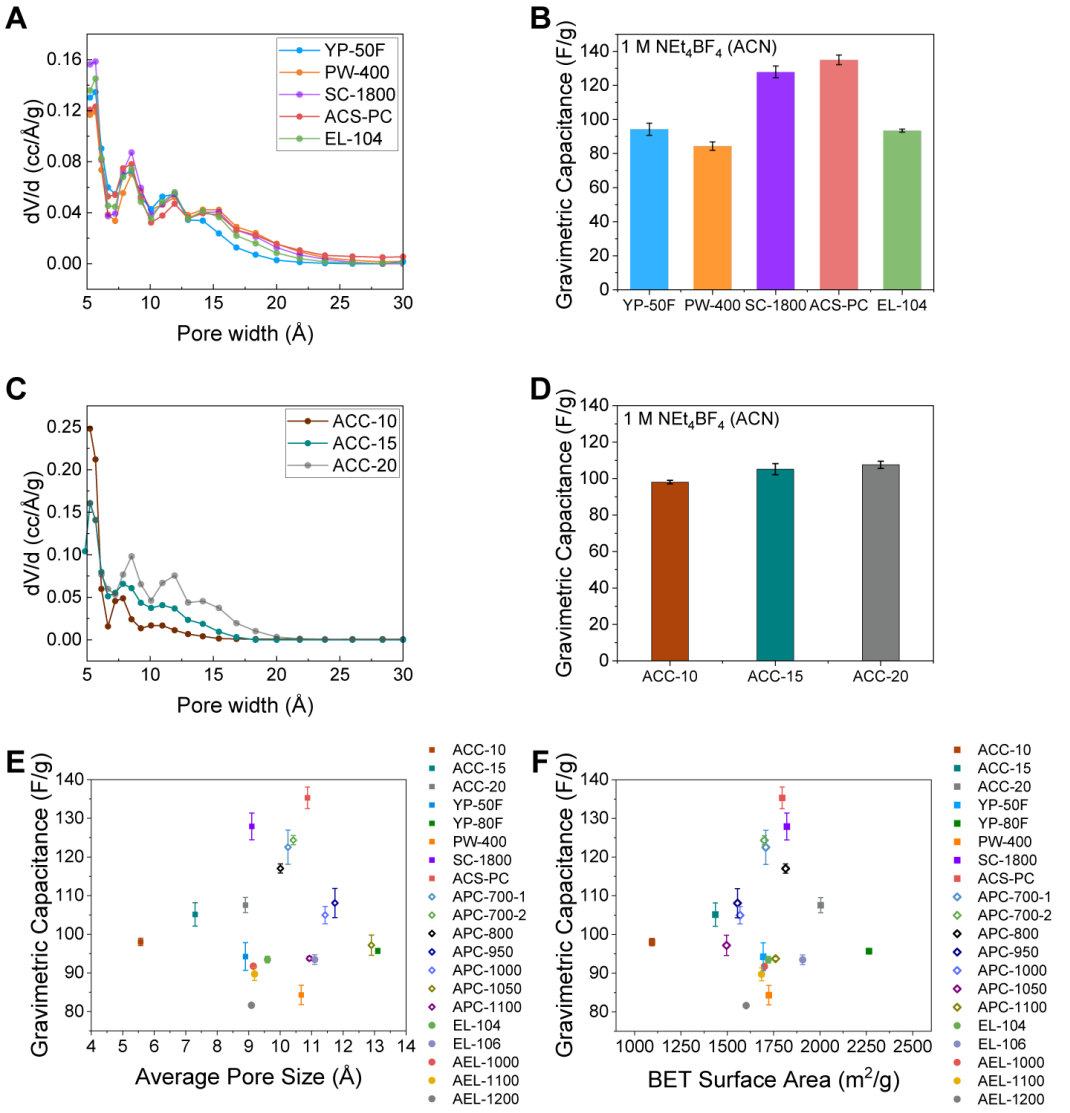

Fig. 1: Relationship between porosity and capacitances for the studied carbons. (**A**) Pore size distributions of five commercial nanoporous carbons calculated based on quenched solid density functional theory analysis (slit pore model) of N_2 isotherms at 77 K (fig. S1) (*23*). (**B**) Gravimetric capacitance of four activated carbons measured at 0.05 A/g in 1 M NEt_4BF_4 (acetonitrile, ACN), error bars represent the standard deviations of repetitive cells (see fig. S4 for data with faster charging currents) (See table S3 for a full list of electrode masses). (**C**) Pore size distributions of three activated carbon cloths. (**D**) Gravimetric capacitance of three activated carbon cloths measured at 0.05 A/g in 1 M NEt_4BF_4 (ACN), (**E**) Relationship between gravimetric capacitance and average pore size of the studied carbons, and (**F**) Relationship between gravimetric capacitance and BET surface area, in addition to the series of 8 commercial carbons. BET surface areas are for carbon powders, rather than film electrodes which also contain PTFE. The latter showed a decrease in BET surface area of ~12% relative to the powder (Fig. S2). In (E) and (F), data are also shown for thermally annealed ACS-PC and EL-104 samples, see later and Methods.

Impact of Local Structural Disorder on Capacitance

As the porosity data fails to explain the wide variations in capacitance, we developed an NMR spectroscopy assay to probe local structural order and its impact on capacitance (Fig. 2). MAS (magic angle spinning) NMR spectra of the studied electrolyte-saturated carbons contain at least two resonances as expected (Fig. 2A). The left-hand resonances, with a similar chemical shift to neat electrolyte are assigned to "ex-pore" anions, including sharp components (free electrolyte) and broad components undergoing exchange with the in-pore environments (*16, 24*). Importantly, the right-hand resonances are assigned to "in-pore" anions, as in previous work (*13-15, 18*). The NMR spectra of the electrolyte-saturated carbons show significant differences, particularly in terms of the $\Delta\delta$ values (table S4, see fig. S9 and S10 for discussion of linewidth and intensity effects). We initially hypothesized that the ion adsorption capacities measured by NMR might correlate with capacitance, but a clear correlation was not found (fig. S10).

However, a correlation is observed between the capacitances and the $\Delta\delta$ values (Fig. 2B, and figs. S9, S11-S15), with carbons possessing $\Delta\delta$ values of smaller magnitude showing higher capacitances. The measured $\Delta\delta$ values are consistent irrespective of the choice of the nucleus probed (fig. S16); *i.e.*, they represent nucleus independent chemical shifts. The $\Delta\delta$ values are therefore indicative of the different structures of the carbons, rather than any specific interactions between the carbons and the studied ions. The correlation of capacitance with $\Delta\delta$ was also observed for ionic liquid electrolytes (fig. S17). The observed correlations are striking given that the carbons were selected from six different independent suppliers and are thus very likely synthesized by a range of different processes/conditions. Since previous studies showed that $\Delta\delta$ values are dominated by domain size effects (rather than pore size effects) for predominantly microporous carbons (*18, 19*), our results further suggest that carbons with smaller ordered domains give rise to higher capacitances.

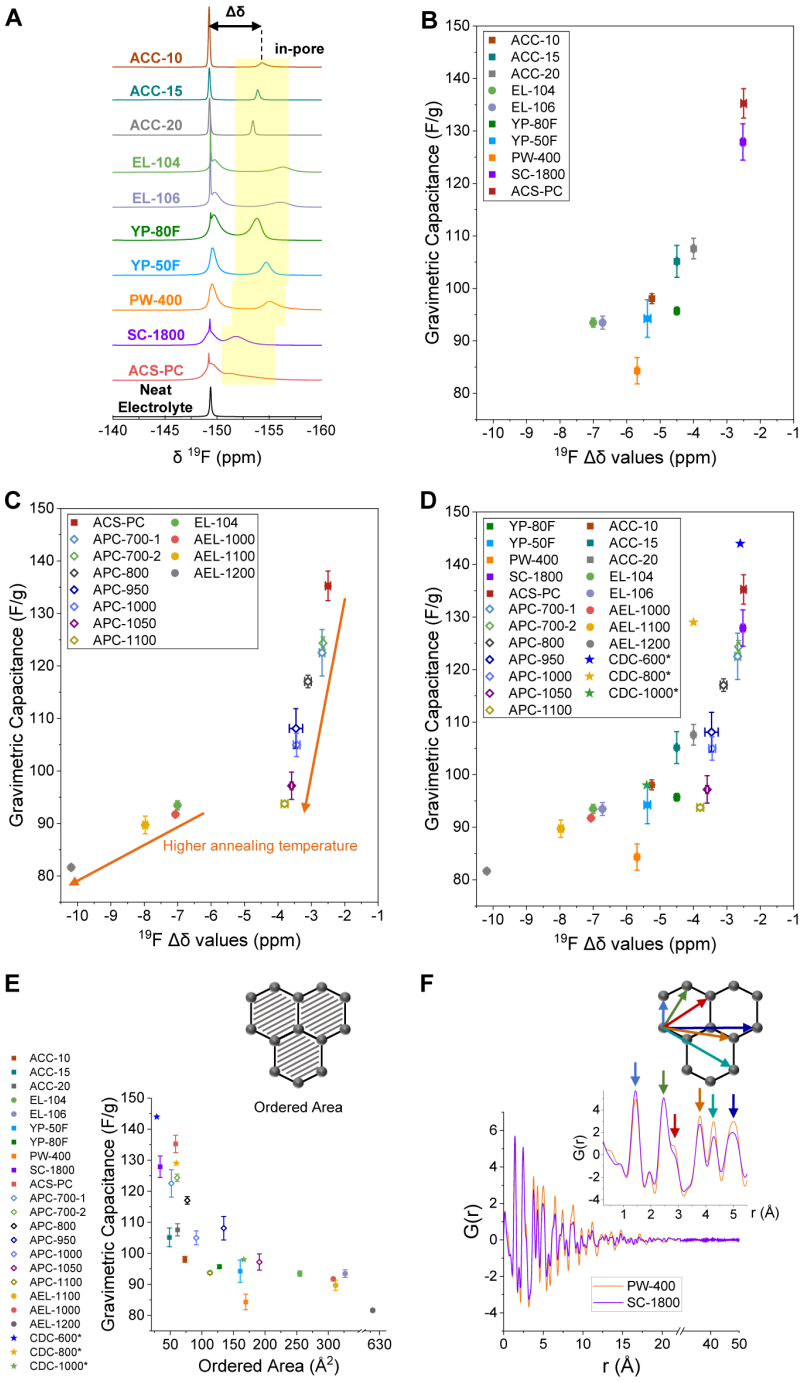

Fig. 2: Characterization of local structural disorder and its correlation with capacitance. (**A**) ^{19}F MAS NMR spectra (9.4 T, 5 kHz MAS) of the studied carbons soaked with 1 M NEt_4BF_4 (ACN). (**B**) Correlation between gravimetric capacitance and ^{19}F Δδ values derived from a), with the in-pore chemical shifts taken as the weighted average for carbons showing multiple in-pore environments. (**C**) Correlation between gravimetric capacitance and ^{19}F Δδ values of thermally annealed ACS-PC and EL-104 samples. (**D**) Correlation between gravimetric capacitance and ^{19}F Δδ values for commercial carbons and thermally annealed carbons, with CDC data also added from previous literature (*3, 18*). (**E**) Correlation between gravimetric capacitance and calculated ordered domain size of the studied carbons. (**F**) Comparison of X-ray PDF plots between two selected carbons: SC-1800 and PW-400. Capacitance values are from constant current charge-discharge measurements at 0.05 A/g in 1 M NEt_4BF_4 (ACN).

To test this hypothesis ACS-PC, the most disordered nanoporous carbons in our series, was thermally annealed at a range of temperatures in argon (see Methods). We hypothesized that thermal annealing would increase structural order in the carbon (*25*), leading to carbons with larger magnitude $\Delta\delta$ values and smaller capacitances. Importantly, gas sorption results were first performed and confirmed that there were minimal changes in the carbon pore structure upon thermal annealing (fig. S18), while XPS measurements revealed a decrease in oxygen content upon annealing (fig. S8). For higher thermal annealing temperatures, $\Delta\delta$ values increase in magnitude as hypothesized, consistent with the formation of carbons with larger ordered domains (Fig. 2C). Furthermore, this increase in structural order was accompanied by a clear decrease in capacitance as hypothesized (Fig. 2C, figs. S3-S6). In addition, EL-104, one of the more ordered carbons in our series, was thermally annealed to explore even more strongly ordered carbon structures (Fig. 2C). Increases in structural order observed by NMR again led to decreases in the capacitance, although less significantly than for ACS-PC, suggesting a limit of lowering the capacitance by increasing the ordered domain sizes for this connected pore system. The consistent observations on annealed carbons further support the hypothesis that it is the local structural disorder that governs the capacitance, rather than pore size (Fig. 2D *vs.* Fig. 1E), with more disordered carbons with smaller ordered domains having higher capacitance. Similar correlations were observed for both gravimetric and volumetric capacitances (Fig. S15).

To further test whether the structural disorder correlates with capacitance, a reported NMR simulation approach was applied to predict the correlation length associated with the size of the ordered aromatic carbon domains (Fig. 2E, see Methods) (*18, 20*). This simulation approach accounts for the experimental pore size distribution and the strength of the ion-carbon interactions; the NMR chemical shifts are then modelled using model polyaromatic hydrocarbon fragments separated by distances governed by the pore size distribution (see Methods). These simulations support the idea that carbons with smaller calculated ordered domain sizes generally have higher capacitances (Fig. 2E). X-ray pair distribution function (PDF) patterns of the studied carbons supported the findings from NMR spectroscopy (Fig. 2F). Comparing the X-ray PDF patterns of SC-1800 (small $\Delta\delta$ value, high capacitance) and PW-400 (large $\Delta\delta$ value, low capacitance), we find that the SC-1800 has a more rapid decay of the pairwise C-C correlations (*18*), consistent with the

smaller domain sizes and/or more the disordered local structure of SC-1800. X-ray PDF results for the other carbons yielded similar results (fig. S19), with a quantitative analysis of the decay rates lending additional support that structural disorder is correlated with capacitance. (fig. S20-S24, table S5).

These findings may help to resolve the previous contradictory reports on the impact of carbon pore size on capacitance (*3, 6-12*). A master plot of our measured Δδ values including literature values for TiC-CDC materials is shown in Fig. 2D. TiC-CDC-600 (*i.e.*, a sample prepared at 600ºC) exhibits a large capacitance and a small Δδ value, while TiC-CDC-1000 has a low capacitance and large Δδ value. This is consistent with a more disordered structure for TiC-CDC-600, as is well known from molecular simulation work (*26, 27*) and conductivity measurements (*3, 28*) that showed an increase in structural order as the synthesis temperature was increased. We therefore hypothesize that carbon disorder was the main factor giving rise to previously reported "anomalous" increase in capacitance for samples prepared at low temperature, although we cannot completely rule out a contribution from porosity, given the narrow pore size distribution of CDCs (*3*). More generally it is possible that the impact of structural disorder has been overlooked in a range of studies on capacitance, and structural disorder should be controlled as far as possible in any study of pore size effects.

Summarizing, our results evidence the idea that disorder in the carbon electrode leads to higher capacitance. While the capacitance data in Figure 2 is for a slow charging rate of 0.05 A g^{-1}, very similar results were obtained at a faster charging rate of 1 A g^{-1} (fig. S6). ACS-PC (a highly disordered carbon) was recorded to have a higher capacitance than the more ordered carbon, EL-104, at the very high charging rate of 10 A g^{-1}, despite the slightly poorer capacitance retention as a function of current for ACS-PC (fig. S6D). Finally, we note that increased disorder may lead to poorer cell cycling stability, depending on the nature of the defects (fig. S6E). The impact of structural disorder on charging rates and cell stability should be explored further in the future.

Impact of Disorder on the Charge Compensation Mechanism

To explore the impact of disorder on the charge storage mechanism, charged supercapacitor electrodes were studied with ex-situ MAS NMR experiments on two selected carbons with contrasting levels of disorder, namely PW-400 (ordered) and SC-1800 (disordered). Magic angle spinning was required to resolve the in-pore peaks due to the small Δδ value for SC-1800, which precluded in-situ measurements. To avoid solvent evaporation during cell disassembly and rotor packing, we employed a 0.5 M PEt_4BF_4 in propylene carbonate (PC) electrolyte, and then used ^{19}F and ^{31}P NMR to study the anions and cations, respectively. Importantly, ex-situ NMR experiments demonstrated excellent reproducibility between independent electrochemical cells (fig. S25, fig. S26).

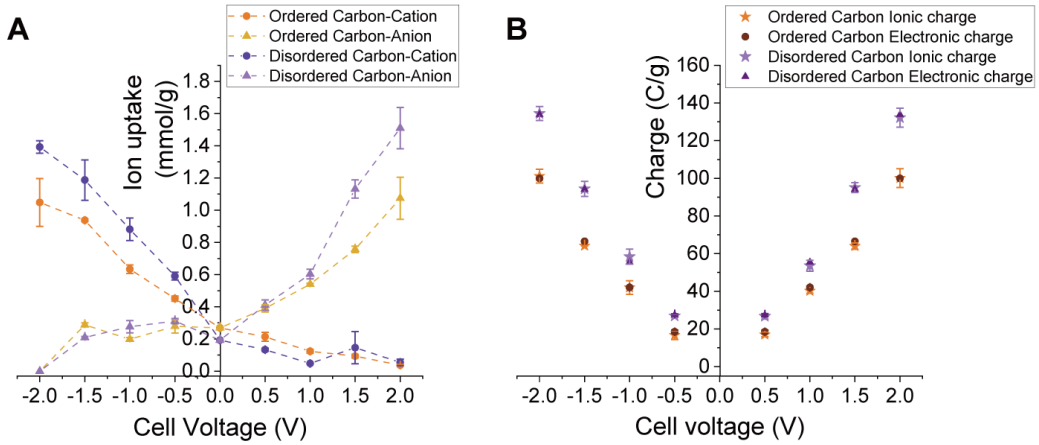

Fig. 3: Charge compensation mechanism of two selected carbons with different local structural disorder. (**A**) Ion uptake of an ordered carbon (PW-400) and a disordered carbon (SC-1800) from ex-situ NMR experiments at different cell voltages (dashed lines were added to guide the eye). See fig. S27 for the NMR spectra and figs. S29, S30 for the spectral deconvolutions. (**B**) Ionic charge of the ordered carbon (PW-400) and disordered carbon (SC-1800) under different cell voltages determined from the in-pore ion population differences, as well electronic charges measured from electrochemistry (see Methods).

The ex-situ NMR measurements report on the number of in-pore cations and anions at different charging voltages (Fig. 3A, fig. S27), as well as the excess ionic charge (Fig. 3B). For both carbons, the anion uptake increases while the cation uptake decreases with increasing applied cell voltage for the positively charged electrodes, and vice versa for the negative electrodes (Fig. 3A). This suggests that both carbons store charge through an ion exchange mechanism, wherein counter ions are adsorbed and co-ions are expelled from the pores for both positive and negative charging (*14*).

Importantly, the more disordered carbon (SC-1800) shows a greater capacity to store ions at a given voltage than the more ordered carbon (PW-400) (Fig. 3B).

We propose that for carbons with smaller domains, the charges are more localized, giving rise to stronger interactions between ions and carbon atoms, thus leading to more efficient storage of ions (fig. S28) (*29, 30*). This capacity to store ions more efficiently leads to higher capacitance for carbons with smaller domains, similar to computational studies on the correlation between capacitance and charge compensation per carbon (*29*). We further hypothesize that the smaller domains may be connected with a higher concentration of topological defects (edge sites, pentagonal and heptagonal rings, curvature), which were previously suggested to increase capacitive performance (*31, 32*). Previous studies of hard carbons for sodium ion batteries found a more favorable interaction of sodium ions with edge sites and defects compared to basal planes of graphene-like fragments (*33, 34*), with the latter paper ascribing the sloping voltage seen in these systems to a pinning of the inserted electrons by the carbon defects (*35*). Finally, while previous studies suggested that carbon-ion distances decrease due to desolvation (*36*), we hypothesize that defects may drive the denser packing of ions in the carbon pores (*37*).

Conclusion and Outlook

In this study we aimed to resolve the debate on how the structure of nanoporous carbons electrodes impacts their capacitive energy storage. Electrochemistry measurements on a large series of commercial activated carbons showed no clear correlation between capacitance and pore size, nor between capacitance and specific surface area. In contrast, NMR spectroscopy experiments and modelling revealed a strong correlation between capacitance and electrode structural disorder for both the commercial porous carbons as well as their thermally annealed counterparts. Carbons with smaller ordered domains have higher capacitances, which we attribute to their more efficient storage of ions in the carbon nanopores. Overall, this work reveals a previously overlooked structural factor that determines the capacitance of nanoporous carbons. may guide the design and synthesis of improved electrode materials for EDLCs.

References and Notes

1. P. Simon, Y. Gogotsi, Perspectives for electrochemical capacitors and related devices. *Nat. Mater.* **19**, 1151-1163 (2020). doi:10.1038/s41563-020-0747-z.
2. H. Shao, Y.-C. Wu, Z. Lin,S P.-L. Taberna, P. Simon, Nanoporous carbon for electrochemical capacitive energy storage. *Chem. Soc. Rev.* **49**, 3005-3039 (2020). doi:10.1039/D0CS00059K.
3. J. Chmiola, G. Yushin, Y. Gogotsi, C. Portet, P. Simon, P. L. Taberna, Anomalous Increase in Carbon Capacitance at Pore Sizes Less Than 1 Nanometer. *Science* **313**, 1760-1763 (2006). doi:10.1126/science.1132195.
4. E. Pomerantseva, F. Bonaccorso, X. Feng, Y. Cui, Y. Gogotsi, Energy storage: The future enabled by nanomaterials. *Science* **366**, eaan8285 (2019). doi:10.1126/science.aan8285.
5. R. Dash, J. Chmiola, G. Yushin, Y. Gogotsi, G. Laudisio, J. Singer, J. Fischer, S. Kucheyev, Titanium carbide derived nanoporous carbon for energy-related applications. *Carbon* **44**, 2489-2497 (2006). doi:10.1016/j.carbon.2006.04.035.
6. C. Largeot, C. Portet, J. Chmiola, P.-L. Taberna, Y. Gogotsi, P. Simon, Relation between the Ion Size and Pore Size for an Electric Double-Layer Capacitor. *J. Am. Chem. Soc.* **130**, 2730-2731 (2008). doi:10.1021/ja7106178.
7. E. Raymundo-Piñero, K. Kierzek, J. Machnikowski, F. Béguin, Relationship between the nanoporous texture of activated carbons and their capacitance properties in different electrolytes. *Carbon* **44**, 2498-2507 (2006). doi:10.1016/j.carbon.2006.05.022.
8. T. A. Centeno, O. Sereda, F. Stoeckli, Capacitance in carbon pores of 0.7 to 15 nm: a regular pattern. *Phys. Chem. Chem. Phys.* **13**, 12403-12406 (2011). doi:10.1039/C1CP20748B.
9. F. Stoeckli, T. A. Centeno, Optimization of the characterization of porous carbons for supercapacitors. *J. Mater. Chem. A* **1**, 6865-6873 (2013). doi:10.1039/C3TA10906B.
10. G. Moreno-Fernandez, S. Perez-Ferreras, L. Pascual, I. Llorente, J. Ibañez, J. M. Rojo, Reply to "Comments on 'Electrochemical study of tetraalkylammonium tetrafluoroborate electrolytes in combination with microporous and mesoporous carbon monoliths' [Electrochimica Acta 268 (2018) 121–130]" by Teresa A.A. Centeno [Electrochim. Acta 296 (2019) 1163–1165]. *Electrochim Acta* **296**, 1166-1167 (2019). doi:10.1016/j.electacta.2018.11.097.
11. L. Suárez, V. Barranco, T. A. Centeno, Impact of carbon pores size on ionic liquid based-supercapacitor performance. *J Colloid Interf Sci* **588**, 705-712 (2021). doi:10.1016/j.jcis.2020.11.093.
12. D.-e. Jiang, Z. Jin, D. Henderson, J. Wu, Solvent Effect on the Pore-Size Dependence of an Organic Electrolyte Supercapacitor. *J. Phys. Chem. Lett.* **3**, 1727-1731 (2012). doi:10.1021/jz3004624.
13. M. Deschamps, E. Gilbert, P. Azais, E. Raymundo-Piñero, M. R. Ammar, P. Simon, D. Massiot, F. Béguin, Exploring electrolyte organization in supercapacitor electrodes with solid-state NMR. *Nat. Mater.* **12**, 351-358 (2013). doi:10.1038/nmat3567.
14. J. M. Griffin, A. C. Forse, H. Wang, N. M. Trease, P.-L. Taberna, P. Simon, C. P. Grey, Ion counting in supercapacitor electrodes using NMR spectroscopy. *Faraday Discuss.* **176**, 49-68 (2014). doi:10.1039/C4FD00138A.
15. A. C. Forse, J. M. Griffin, C. Merlet, P. M. Bayley, H. Wang, P. Simon, C. P. Grey, NMR Study of Ion Dynamics and Charge Storage in Ionic Liquid Supercapacitors. *J. Am. Chem. Soc.* **137**, 7231-7242 (2015). doi:10.1021/jacs.5b03958.

16. L. Cervini, N. Barrow, J. Griffin, Observing Solvent Dynamics in Porous Carbons by Nuclear Magnetic Resonance : Elucidating molecular-level dynamics of in-pore and ex-pore species. *Johnson Matthey Technol. Rev.* **64**, 152-164 (2020). doi:10.1595/205651320X15747624015789.
17. R. K. Harris, T. V. Thompson, P. R. Norman, C. Pottage, Phosphorus-31 NMR studies of adsorption onto activated carbon. *Carbon* **37**, 1425-1430 (1999). doi:10.1016/S0008-6223(99)00004-4.
18. A. C. Forse, C. Merlet, P. K. Allan, E. K. Humphreys, J. M. Griffin, M. Aslan, M. Zeiger, V. Presser, Y. Gogotsi, C. P. Grey, New Insights into the Structure of Nanoporous Carbons from NMR, Raman, and Pair Distribution Function Analysis. *Chem. Mater.* **27**, 6848-6857 (2015). doi:10.1021/acs.chemmater.5b03216.
19. A. C. Forse, J. M. Griffin, V. Presser, Y. Gogotsi, C. P. Grey, Ring Current Effects: Factors Affecting the NMR Chemical Shift of Molecules Adsorbed on Porous Carbons. *J. Phys. Chem. C* **118**, 7508-7514 (2014). doi:10.1021/jp502387x.
20. C. Merlet, A. C. Forse, J. M. Griffin, D. Frenkel, C. P. Grey, Lattice simulation method to model diffusion and NMR spectra in porous materials. *J. Chem. Phys.* **142**, 094701 (2015). doi:10.1063/1.4913368.
21. A. Sasikumar, J. M. Griffin, C. Merlet, Understanding the Chemical Shifts of Aqueous Electrolyte Species Adsorbed in Carbon Nanopores. *J. Phys. Chem. Lett.* **13**, 8953–8962 (2022). doi:10.1021/acs.jpclett.2c02260.
22. Y.-Z. Xing, Z.-X. Luo, A. Kleinhammes, Y. Wu, Probing carbon micropore size distribution by nucleus independent chemical shift. *Carbon* **77**, 1132-1139 (2014). doi:10.1016/j.carbon.2014.06.031.
23. G. Y. Gor, M. Thommes, K. A. Cychosz, A. V. Neimark, Quenched solid density functional theory method for characterization of mesoporous carbons by nitrogen adsorption. *Carbon* **50**, 1583-1590 (2012). doi:10.1016/j.carbon.2011.11.037.
24. N. Fulik, F. Hippauf, D. Leistenschneider, S. Paasch, S. Kaskel, E. Brunner, L. Borchardt, Electrolyte mobility in supercapacitor electrodes - Solid state NMR studies on hierarchical and narrow pore sized carbons. *Energy Storage Mater.* **12**, 183-190 (2018). doi:10.1016/j.ensm.2017.12.008.
25. H. Yin, H. Shao, B. Daffos, P.-L. Taberna, P. Simon, The effects of local graphitization on the charging mechanisms of microporous carbon supercapacitor electrodes. *Electrochem. Commun.* **137**, 107258 (2022). doi:10.1016/j.elecom.2022.107258.
26. P. Zetterstrom, S. Urbonaite, F. Lindberg, R. G. Delaplane, J. Leis, G. Svensson, Reverse Monte Carlo studies of nanoporous carbon from TiC. *J. Phys. Condens. Matter* **17**, 3509-3524 (2005). doi:10.1088/0953-8984/17/23/004.
27. J. C. Palmer, A. Llobet, S. H. Yeon, J. E. Fischer, Y. Shi, Y. Gogotsi, K. E. Gubbins, Modeling the structural evolution of carbide-derived carbons using quenched molecular dynamics. *Carbon* **48**, 1116-1123 (2010). doi:10.1016/j.carbon.2009.11.033.
28. B. Dyatkin, Y. Gogotsi, Effects of structural disorder and surface chemistry on electric conductivity and capacitance of porous carbon electrodes. *Faraday Discuss.* **172**, 139-162 (2014). doi:10.1039/c4fd00048j.
29. Y. M. Liu, C. Merlet, B. Smit, Carbons with Regular Pore Geometry Yield Fundamental Insights into Supercapacitor Charge Storage. *ACS Cent. Sci.* **5**, 1813-1823 (2019). doi:10.1021/acscentsci.9b00800.

30. C. Merlet, C. Pean, B. Rotenberg, P. A. Madden, B. Daffos, P. L. Taberna, P. Simon, M. Salanne, Highly confined ions store charge more efficiently in supercapacitors. *Nat. Comm.* **4**, 2701 (2013). doi:10.1038/ncomms3701.
31. J. F. Chen, Y. L. Han, X. H. Kong, X. Z. Deng, H. J. Park, Y. L. Guo, S. Jin, Z. K. Qi, Z. Lee, Z. H. Qiao, R. S. Ruoff, H. X. Ji, The Origin of Improved Electrical Double-Layer Capacitance by Inclusion of Topological Defects and Dopants in Graphene for Supercapacitors. *Angew. Chem. Int. Ed.* **55**, 13822-13827 (2016). doi:10.1002/anie.201605926.
32. J. W. Zhu, Y. P. Huang, W. C. Mei, C. Y. Zhao, C. T. Zhang, J. Zhang, I. S. Amiinu, S. C. Mu, Effects of Intrinsic Pentagon Defects on Electrochemical Reactivity of Carbon Nanomaterials. *Angew. Chem. Int. Ed.* **58**, 3859-3864 (2019). doi:10.1002/anie.201813805.
33. A. Vasileiadis, Y. Q. Li, Y. X. Lu, Y. S. Hu, M. Wagemaker, Role of Defects, Pores, and Interfaces in Deciphering the Alkali Metal Storage Mechanism in Hard Carbon. *ACS Appl. Energy Mater.* **6**, 127-140 (2023). doi:10.1021/acsaem.2c02591.
34. V. L. Deringer, C. Merlet, Y. C. Hu, T. H. Lee, J. A. Kattirtzi, O. Pecher, G. Csányi, S. R. Elliott, C. P. Grey, Towards an atomistic understanding of disordered carbon electrode materials. *Chem. Comm.* **54**, 5988-5991 (2018). doi:10.1039/c8cc01388h.
35. J. M. Stratford, P. K. Allan, O. Pecher, P. A. Chater, C. P. Grey, Mechanistic insights into sodium storage in hard carbon anodes using local structure probes. *Chem. Comm.* **52**, 12430-12433 (2016). doi:10.1039/c6cc06990h.
36. J. Chmiola, C. Largeot, P. L. Taberna, P. Simon, Y. Gogotsi, Desolvation of ions in subnanometer pores and its effect on capacitance and double-layer theory. *Angew. Chem. Int. Ed.* **47**, 3392-3395 (2008). doi:10.1002/anie.200704894.
37. E. Lee, K. A. Persson, Li Absorption and Intercalation in Single Layer Graphene and Few Layer Graphene by First Principles. *Nano Lett.* **12**, 4624-4628 (2012). doi:10.1021/nl3019164.
38. X. Y. Liu, D. X. Lyu, C. Merlet, M. Leesmith, X. Hua, Z. Xu, C. P. Grey, A. C. Forse, Research Data supporting "Structural Disorder Determines Capacitance in Nanoporous Carbons". *Cambridge Research Repository, Apollo*, (2023). doi:10.17863/CAM.104594.
39. D. A. Gomez-Gualdron, P. Z. Moghadam, J. T. Hupp, O. K. Farha, R. Q. Snurr, Application of Consistency Criteria To Calculate BET Areas of Micro- And Mesoporous Metal-Organic Frameworks. *J. Am. Chem. Soc.* **138**, 215-224 (2016). doi:10.1021/jacs.5b10266.
40. L. M. Dickinson, R. K. Harris, J. A. Shaw, M. Chinn, P. R. Norman, Oxygen-17 and deuterium NMR investigation into the adsorption of water on activated carbon. *Magn. Reson. Chem.* **38**, 918-924 (2000). doi:10.1002/1097-458x(200011)38:11<918::Aid-Mrc749>3.0.Co;2-7.
41. A. Belhboub, E. Lahrar, P. Simon, C. Merlet, On the development of an original mesoscopic model to predict the capacitive properties of carbon-carbon supercapacitors. *Electrochim Acta* **327**, 135022 (2019). doi:10.1016/j.electacta.2019.135022.
42. A. Sasikumar, A. Belhboub, C. Bacon, A. C. Forse, J. M. Griffin, C. P. Grey, P. Simon, C. Merlet, Mesoscopic simulations of the NMR spectra of porous carbon based supercapacitors: electronic structure and adsorbent reorganisation effects. *Phys. Chem. Chem. Phys.* **23**, 15925-15934 (2021). doi:10.1039/d1cp02130c.
43. M. L. P. Price, D. Ostrovsky, W. L. Jorgensen, Gas-phase and liquid-state properties of esters, nitriles, and nitro compounds with the OPLS-AA force field. *J. Comput. Chem.* **22**, 1340-1352 (2001). doi:DOI 10.1002/jcc.1092.
44. J. N. C. Lopes, A. A. H. Pádua, Molecular force field for ionic liquids composed of triflate or

bistriflylimide anions. *J. Phys. Chem. B* **108**, 16893-16898 (2004). doi:10.1021/jp0476545.

45. J. N. C. Lopes, A. A. H. Pádua, Molecular force field for ionic liquids III:: Imidazolium, pyridinium, and phosphonium cations;: Chloride, bromide, and dicyanamide anions. *J. Phys. Chem. B* **110**, 19586-19592 (2006). doi:10.1021/jp063901o.
46. M. W. Cole, J. R. Klein, The Interaction between Noble-Gases and the Basal-Plane Surface of Graphite. *Surf. Sci.* **124**, 547-554 (1983). doi:10.1016/0039-6028(83)90808-7.
47. S. Plimpton, Fast Parallel Algorithms for Short-Range Molecular-Dynamics. *J. Comput. Phys.* **117**, 1-19 (1995). doi:DOI 10.1006/jcph.1995.1039.
48. G. W. T. M. J. Frisch, H. B. Schlegel, G. E. Scuseria, M. A. Robb, J. R. Cheeseman, G. Scalmani, V. Barone, B. Mennucci, G. A. Petersson, H. Nakatsuji, M. Caricato, X. Li, H. P. Hratchian, A. F. Izmaylov, J. Bloino, G. Zheng, J. L. Sonnenberg, M. Hada, M. Ehara, K. Toyota, R. Fukuda, J. Hasegawa, M. Ishida, T. Nakajima, Y. Honda, O. Kitao, H. Nakai, T. Vreven, J. A. Montgomery, Jr., J. E. Peralta, F. Ogliaro, M. Bearpark, J. J. Heyd, E. Brothers, K. N. Kudin, V. N. Staroverov, R. Kobayashi, J. Normand, K. Raghavachari, A. Rendell, J. C. Burant, S. S. Iyengar, J. Tomasi, M. Cossi, N. Rega, J. M. Millam, M. Klene, J. E. Knox, J. B. Cross, V. Bakken, C. Adamo, J. Jaramillo, R. Gomperts, R. E. Stratmann, O. Yazyev, A. J. Austin, R. Cammi, C. Pomelli, J. W. Ochterski, R. L. Martin, K. Morokuma, V. G. Zakrzewski, G. A. Voth, P. Salvador, J. J. Dannenberg, S. Dapprich, A. D. Daniels, Ö. Farkas, J. B. Foresman, J. V. Ortiz, J. Cioslowski, and D. J. Fox,. (Wallingford, CT, 2013).
49. X. Qiu, J. W. Thompson, S. J. L. Billinge, PDFgetX2: a GUI-driven program to obtain the pair distribution function from X-ray powder diffraction data. *J. Appl. Crystallogr.* **37**, 678 (2004). doi:10.1107/S0021889804011744.
50. Takeshi Egami, S. J. L. Billinge, *Underneath the Bragg Peaks Structural Analysis of Complex Materials*. (Pergamon, 2012).
51. L. Borchardt, M. Oschatz, S. Paasch, S. Kaskel, E. Brunner, Interaction of electrolyte molecules with carbon materials of well-defined porosity: characterization by solid-state NMR spectroscopy. *Phys. Chem. Chem. Phys.* **15**, 15177-15184 (2013). doi:10.1039/c3cp52283k.

365

Acknowledgements

We acknowledge Mengnan Wang, Dr Jesús Barrio, Angus Pedersen and Prof. Magdalena Titirici for the XPS measurements at Imperial College London. We acknowledge James Gittins for conducting the N_2 gas sorption analysis of the YP-80F carbon film. We also acknowledge Dr. Nathan Halcovitch for optimizing the X-ray diffractometer to collect the total scattering data. This work was granted access to the HPC resources of the CALMIP supercomputing centre under the allocation P21014.

Funding: X. L. is supported PhD funding from the Cambridge Trust and the China Scholarship Council. This work was supported by a UKRI Future Leaders Fellowship to A. C. F. (MR/T043024/1), which also supported Z. X. This project was supported by funding to C. M. from the European Research Council (ERC) under the European Union's Horizon 2020 research and innovation program (grant agreement no. 714581). M. L. and X. H. acknowledge the support from a Research Grant via the Royal Society (GS\R2\222222) and a Research Enablement Grant via the Royal Society of Chemistry (E22-8441857550). D.L. acknowledges the China Scholarship Council (CSC) and Cambridge Trust Scholarship.

Author contributions: A. C. F. and C. P. G. supervised and guided the project. A. C. F., C. P. G. and X. L. designed the research. X. L. completed the electrode fabrication, cell assembly, N_2 sorption, electrochemical measurements, NMR experiments and data analysis. D. L. helped analyze the NMR results. C. M. performed the NMR simulations and interpreted the results. M. L. and X. H. performed XPDF experiments and analyzed the data. Z. X. analyzed the XPS results. X. L. and A. C. F. drafted the manuscript, and all authors contributed to the manuscript revision.

Completing interests: Authors declare that they have no competing interests.

Data and materials availability: All data are available in the main text or the supplementary materials. All raw experimental data files are available in the Cambridge Research Repository, Apollo (*38*) .

Supplementary Materials

Materials and Methods
Figs. S1 to S32
Tables S1 to S5
References (39-51)